Structure of the bacterial flagellar protofilament and implications for a switch for supercoiling

Fadel A. Samatey*, Katsumi Imada*, Shigehiro Nagashima*, Ferenc Vonderviszt†, Takashi Kumasaka‡, Masaki Yamamoto‡ & Keiichi Namba*§

* *Protonic NanoMachine Project, ERATO, JST, 3-4 Hikaridai, Seika, Kyoto 619-0237, Japan*
† *Department of Physics, University of Veszprém, Egyetem, u.10 H-8201, Hungary*
‡ *RIKEN Harima Institute, 1-1-1 Kouto, Mikazuki, Hyogo 679-5198, Japan*
§ *Advanced Technology Research Laboratories, Matsushita Electric Industrial Co., Ltd, 3-4 Hikaridai, Seika, Kyoto 619-0237, Japan*

The bacterial flagellar filament is a helical propeller constructed from 11 protofilaments of a single protein, flagellin. The filament switches between left- and right-handed supercoiled forms when bacteria switch their swimming mode between running and tumbling. Supercoiling is produced by two different packing interactions of flagellin called L and R. In switching from L to R, the intersubunit distance (~52 Å) along the protofilament decreases by 0.8 Å. Changes in the number of L and R protofilaments govern supercoiling of the filament. Here we report the 2.0 Å resolution crystal structure of a *Salmonella* flagellin fragment of relative molecular mass 41,300. The crystal contains pairs of antiparallel straight protofilaments with the R-type repeat. By simulated extension of the protofilament model, we have identified possible switch regions responsible for the bi-stable mechanical switch that generates the 0.8 Å difference in repeat distance.

Bacteria swim by rotating helical flagellar filaments, which are up to 15 μm long, but only 120–250 Å in diameter. The rotary motor at the base of the filament drives the rotation of this helical propeller[1,2] at hundreds of revolutions per second[3,4]. For chemotaxis and thermotaxis, the swimming pattern of bacteria such as *Salmonella* and *Escherichia coli* alternates between 'run' and 'tumble'; a run lasts for a few seconds and a tumble for a fraction of second. During a run, the motor rotates counterclockwise (as it is viewed from outside the cell), and several flagellar filaments with a left-handed helical shape form a bundle and propel the cell. A tumble is caused by quick reversal of the motor to clockwise rotation[5], which produces a twisting force that transforms the left-handed helical form of the filament into a right-handed one[6,7], causing the bundle to fall apart rapidly. The separated filaments act in an uncoordinated way to generate forces that change the orientation of the cell. Thus, the structure of the flagellar filament and its dynamic properties have an essential role in bacterial taxis.

The filament is a helical assembly of a single protein, flagellin, with roughly 11 subunits per 2 turns of the 1-start helix; the filament can also be described as a tubular structure comprising 11 strands of protofilaments, which are nearly longitudinal helical arrays of subunits[8]. The helical forms of the filament are caused by supercoiling, which is proposed to occur through a switching of conformation or packing interactions of the subunits between two distinct states and their non- and quasi-equivalent intersubunit interactions[9–12]. In the proposed models, each protofilament exists in one of two slightly different conformations, which affect the repeat distance and lateral packing interaction; the regulated switching of the 11 protofilaments would then produce ten types of supercoil and two types of straight filament.

Many of these forms have actually been observed in various strains and under various conditions[13–15]. The two straight filaments are called L-type and R-type according to the left- and right-handed twist of the protofilaments, respectively[16]. Accurate measurements by X-ray fibre diffraction show that the repeat distances of the L- and R-type protofilaments are 52.7 Å and 51.9 Å, respectively, the difference being only 0.8 Å. A simple mechanical simulation of supercoiled forms with these structural parameters shows a good agreement with the pitch and diameter of observed supercoils, indicating that the data and the model are both physically sound[17]. This also indicates that the level of precision at which flagellin works as a lengthwise mechanical switch is on the order of a tenth of an ångstrom.

Electron cryomicroscopy and X-ray fibre diffraction have revealed the domain organization of flagellin and subunit packing in the two types of straight filaments at about 10 Å resolution[17–22]; however, higher resolution is needed to understand the structural basis of supercoiling in atomic detail. Here we present the crystal structure of the flagellin F41 fragment (relative molecular mass (M_r) 41,300 (41K)) at 2.0 Å resolution, which directly reveals the protofilament structure. A portion of the F41 molecule involved in the axial subunit packing is associated with conformational switching, providing insights into a mechanical switch that works with sub-ångstrom precision.

Structure of F41

Because flagellin polymerizes into filaments, evading crystallization efforts, we prepared and crystallized a 41K fragment of *Salmonella* flagellin by clipping off peptides from both the amino- and carboxy-terminal ends. Although the crystals were only several micrometres thick, various improvements in the cryocrystallographic technique[23] allowed data collection at ESRF and SPring-8, resulting in a refined atomic model at 2.0 Å resolution.

The Cα backbone trace of F41 is shown in Fig. 1a. The overall shape of the molecule looks like a boomerang or an aircraft with two wings and a short body, each wing being about 70 Å long, 25 Å wide and 20 Å thick. The F41 structure can be divided into three domains, labelled D1, D2 and D3. Domain D1 comprises an N-terminal segment from Asn 56 to Gln 176, and a C-terminal segment from Thr 402 to Arg 450. Domain D2 also comprises two segments: Lys 177 to Gly 189, and Ala 284 to Ala 401. A central segment from Tyr 190 to Val 283 makes up domain D3. The domains are connected by short stretches of two chains in both cases. A cross β-motif is used to tie up the two ends of domain D1 connecting to

D2, where two hydrogen bonds are formed between Asn 173 and Thr 404. The two chains connecting domains D2 and D3, Gly 189 to Thr 193 and Val 281 to Asn 285, form a short β-strand. The distribution of domains and secondary structures along the amino-acid sequence is summarized in Fig. 1c.

Domain D1 is rod shaped, about 70 Å long and 20 Å wide, and comprises three α-helices and a strand of a unique β-turn/β-hairpin/α-helix motif. The N-terminal chain forms two α-helices and a β-hairpin. The first α-helix (residues 57–99) extends through the long axis of this domain, and the second one is relatively short (104–129). The β-hairpin (140–160), with a small crossed loop at its tip (146–153), is flanked by two distorted β-turns (131–134 and 135–138) on the N-terminal side, and slightly more than one turn of α-helix (163–168) on the C-terminal side. This α-helix is followed by an extended chain (170–176). The C-terminal chain forms an α-helix (406–447) as long as the first N-terminal α-helix. This rod-shaped domain forms an extensive hydrophobic core along its central axis in a similar way to four-helix bundles in other protein structures. But, because of an irregularity in one of the four strands involving the β-turn/β-hairpin/α-helix in series, the packing of hydrophobic side chains is relatively loose in the middle portion (Fig. 1b).

Domain D2 is made up of mostly β-strands except for one short 3_{10} helix (285–289) and one short α-helix (288–298). The fold of a set of these β-strands is unique and best described as a series of randomly oriented β-hairpins, with some of them also involved in three-stranded β-sheets. This domain has three distinct hydrophobic regions, two of which form enclosed hydrophobic cores; therefore, domain D2 can be divided into two compact subdomains, D2a and D2b (Fig. 1b).

Subdomain D2a consists of the N-terminal stretch (177–189) and the first half of the C-terminal segment (284–344) of domain D2. Its hydrophobic core comprising 12 side chains is enclosed in a slightly irregular and unusual barrel formed by four β-strands and one α-helix. Subdomain D2b is formed by the last half of the C-terminal segment (345–401) of domain D2. Its hydrophobic core is relatively small, consisting of six side chains that are enclosed within the palm of a right-hand glove made of two β-hairpins corresponding to the thumb and forefinger and a loop corresponding to the remaining three fingers.

These two subdomains form domain D2 by intimate interactions between their hydrophobic surfaces. The third hydrophobic region of domain D2 is formed as part of this interface. These hydrophobic interactions between the two subdomains might explain why a proteolytic fragment composed of domains D2 and D3 behaves as two cooperatively unfolding domains instead of three in calorimetric analyses[24,25].

Domain D3 also consists of mostly β-strands with one short stretch of a helical fold (199–209); however, this helical stretch does not have the regular hydrogen-bonding pattern of an α-helix or a 3_{10}-helix. Domain D3 can be regarded as an unusual barrel made of four β-strands and one helical strand, which encloses 15 hydrophobic side chains in its core (Fig. 1a, b). This fold is similar to a part of D2a described above, and in addition a section of this fold can be described as a series of randomly oriented β-hairpins. Flagellin can have domain D3 deleted without losing its ability to form filaments, although the filaments are significantly more unstable than those of wild-type flagellin[26]. The relatively independent arrangement of this domain from the rest explains why its deletion has a minimal effect on the structural integrity of flagellin. The reduction in the filament stability is due to the loss of intersubunit interactions, as shown by an electron microscopic study[22].

In domains D2 and D3, the Cα backbone trace shows a previously undescribed fold. Three portions with this fold are isolated and

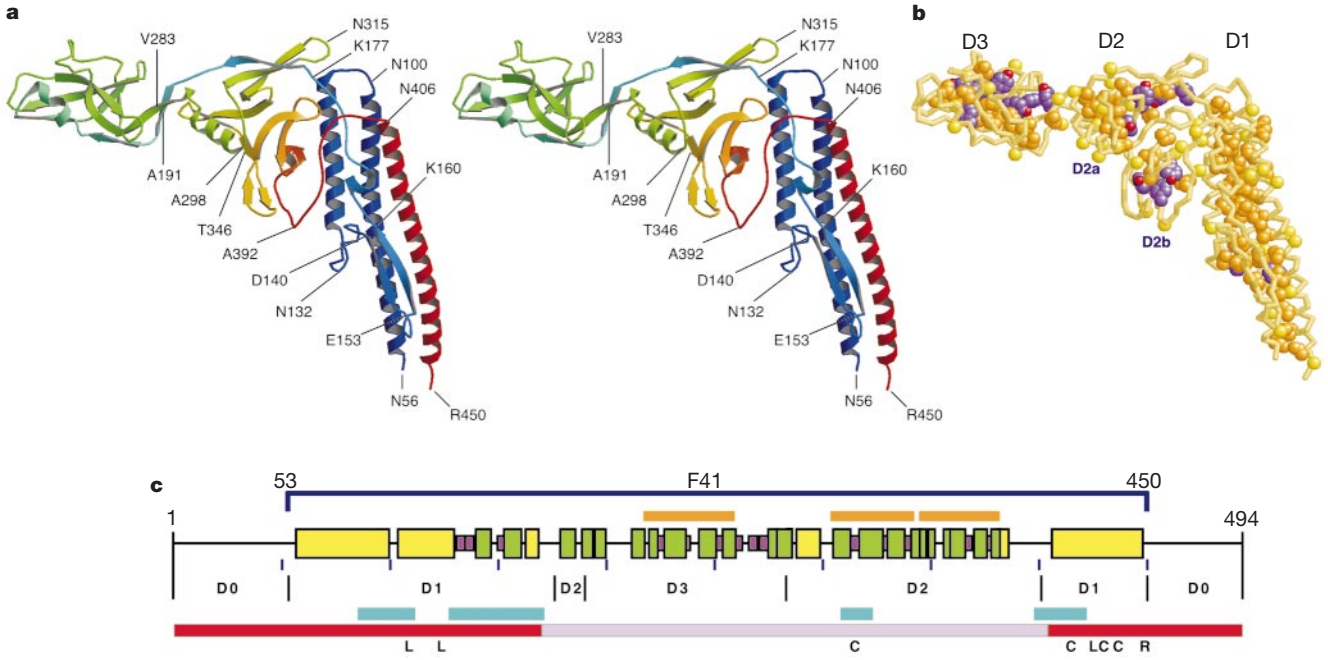

Figure 1 The Cα backbone trace, hydrophobic core distribution and structural information of F41. **a**, Stereo diagram of the Cα backbone. The chain is colour coded from blue to red from the N to the C terminus. Prepared with MOLSCRIPT[44] and RASTER3D[45]. **b**, Four distinct hydrophobic cores that define domains D1, D2a, D2b and D3. All the hydrophobic side-chain atoms are displayed with the Cα backbone. Side-chain atoms are colour coded: Ala, yellow; Leu, Ile or Val, orange; Phe and Tyr, purple (carbon atoms) and red (oxygen atoms). Prepared with RASMOL[46]. **c**, Position and region of various structural features in the amino-acid sequence of flagellin. Shown are, from top to bottom: the F41 fragment in blue; three β-folium folds in brown; the secondary structure distribution with α-helix in yellow, β-structure in green, and β-turn in purple; tic mark at every 50th residue in blue; domains D0, D1, D2 and D3; the axial subunit contact region within the protofilament in cyan; the well-conserved amino-acid sequence in red and variable region in violet; point mutations in F41 that produce the filaments of different supercoils. Letters at the bottom indicate the morphology of mutant filaments: L (D107E, R124A, R124S, G426A), L-type straight; R (A449V), R-type straight; C (D313Y, A414V, A427V, N433D), curly[33].

shown in Fig. 2 (corresponding regions of the amino-acid sequence are indicated in Fig. 1c). The fold comprises a series of β-hairpins all pointing away from one another like three thin leaves spread out or like a curve of cubic polynomial called the 'folium of Descartes'. We therefore named it the β-folium. A common feature found in these β-foliums is that most of the tips of β-hairpins are either bent or twisted, and so some of them are better described as a β-finger with a claw.

Structure of the protofilament

The flagellar filament is made of 11 protofilaments all with the same polarity. From fibre-diffraction studies, two distinct subunit repeat distances along the protofilament have been identified as L- and R-type[16]. More accurate measurements have determined that the L-type repeat is 52.7 Å and the R-type repeat is 51.9 Å, with experimental errors smaller than 0.1 Å (ref. 17). The repeat distance along the *a* axis of the F41 crystal is 51.8 Å (± 0.1 Å), which encouraged us to look for the protofilament structure in the crystal as soon as the electron density map became available. As expected, we found that the protofilament structure with F41 molecules lined up along the *a* axis in the same orientation. The overall shape of the protofilament looks exactly the same as those found in lower resolution density maps obtained by electron cryomicroscopy[18,19].

The molecular packing in the crystal is shown in Fig. 3 in two orthogonal views. Because the crystal has a space group of $P2_1$, two perfectly straight protofilaments are packed antiparallel and this pair repeats along the *b* axis every 36.5 Å, forming a flat sheet. This mode of molecular packing is the same as that found in the zinc sheet of tubulin, in which the protofilaments of microtubule form an antiparallel array within the monolayer sheet[27]. The flagellar protofilaments formed a stack of sheets up to a few hundred layers with a repeat of 119 Å, producing three-dimensional, plate crystals that were several micrometres thick.

The atomic model of one protofilament from the F41 crystal structure was relatively easily docked onto a low-resolution density map of the R-type straight filament from electron cryomicroscopy and fibre diffraction[17,18] (Fig. 4). The fit is nearly perfect for a few consecutive subunits, clearly showing that the protofilament structure in the crystal is almost identical to that in the filament. Although the protofilament model is straight and the corresponding protofilament density is gently wound into a right-handed helix, the twist and curvature of this helix are very small.

Three of the four domains identified previously in the filament density map, D1, D2 and D3 (named in the order of their radial positions from inside to outside), correspond with the three domains identified in the F41 structure. Domain D1 of the F41 atomic model is located in the outer-tube region of the filament (Fig. 4, OT), filling most of the outer-tube volume, but not the inner-tube region (Fig. 4, IT). This indicates that a large portion of the truncated terminal regions from Ala 1 to Arg 52 and from Ser 451 to Arg 494, which are unfolded in the monomeric form, occupies the inner-tube volume. Domains D2 and D3 respectively fill the two outer domains of the density map. These observations are consistent with previous amino-acid assignments of the domains[17,18,20–22,28], with slight corrections to the domain boundaries (Fig. 1c). The nearly axial alignment of long α-helices in the outer-tube region matches the original predictions from X-ray fibre diffraction data[29].

The outer-tube domain is known to be solely responsible for the formation of two distinct helical lattices, L-type and R-type[20]. Even when the inner-tube structures are removed by truncating the terminal segments, flagellin fragments can polymerize into supercoiled filaments if seeded by the wild-type supercoiled filaments[30]. This means that the outer-tube domain D1 has the ability to switch between the two states of flagellin represented by the L-type and R-type straight filament structures.

The protofilament of the R-type repeat is held in the crystal by axial interactions between D1 domains, and it exists in the absence of lateral protofilament interactions that construct the flagellar filament. This indicates that each protofilament is an independent, cooperatively switching unit, at least for the lengthwise mechanical switch that produces the curvatures of supercoiled filaments by incorporating the two types of protofilament into the tubular structure. This also indicates that the axial intersubunit interactions

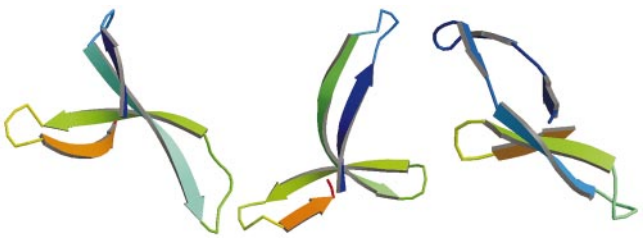

Figure 2 The β-folium fold. Left, residues 220–260 in domain D3; middle, residues 308–345 in domain D2a; right, residues 345–383 in domain D2b. The chain is colour coded from blue to green to brown according to the amino-acid sequence. Prepared with MOLSCRIPT[44] and RASTER3D[45].

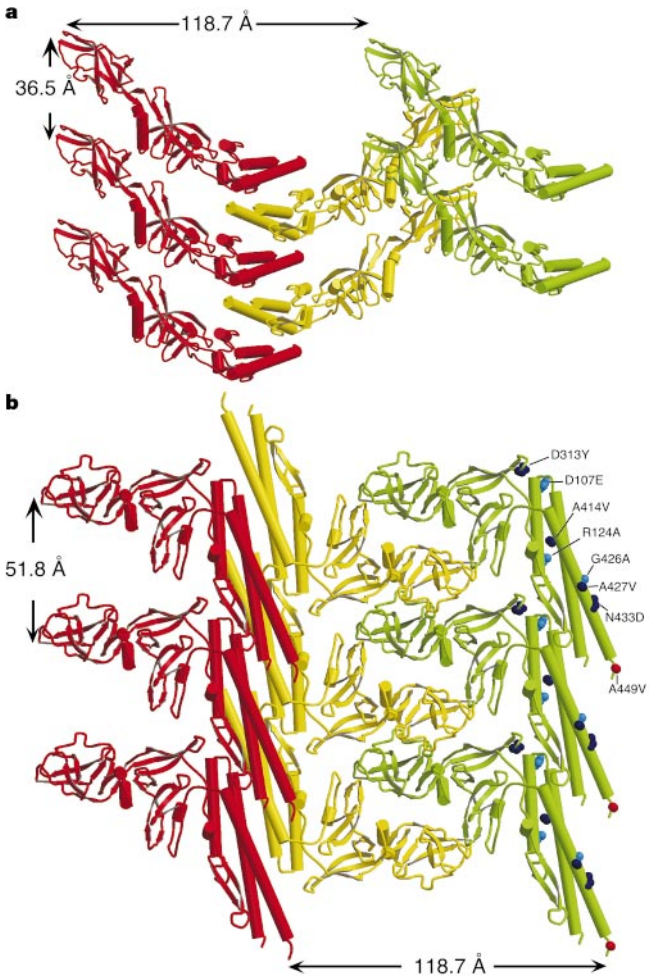

Figure 3 Crystal packing of F41 in two orthogonal views. **a**, The *b*–*c* plane viewed down the *a* axis. **b**, The *a*–*c* plane viewed down the *b* axis. Each array of the F41 molecules along the *a* axis, which has been identified as the protofilament of the flagellar filament, is coloured red, yellow and green. The repeat distances are labelled. Antiparallel packing of the protofilaments by the $P2_1$ symmetry of the crystal is clearly shown. Mutation sites that affect the supercoiling are also labelled with side-chain atoms shown in CPK representation. Mutations are coloured blue for L-type, red for R-type, and black for curly. Prepared with MOLSCRIPT[44] and RASTER3D[45].

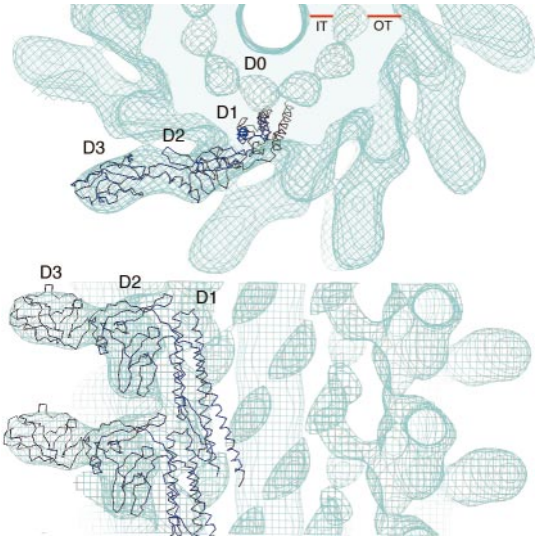

Figure 4 Docking of a single protofilament model into the density map of the filament. Top panel, end-on view from the top, with a 50 Å thick cross-section of the map. The map is painted where the density is higher than the contour level. Bottom panel, side view, with a 50 Å thick longitudinal section of the map that spans from the filament axis towards readers. The top points towards the distal end of the flagellum. The resolution of the density map was limited to 20 Å for easy evaluation of the model fitting. D0, D1, D2 and D3 indicate the domains of flagellin; IT and OT represent the inner- and outer-tube regions, respectively. Prepared with O[41].

between D1 domains along the protofilament are responsible for the two-state switching to produce the two distinct repeat distances.

Axial interactions within the protofilament

The axial intersubunit interactions are formed between domain D1 of the upper subunit and domain D1 and a small portion of D2a of the lower subunit (Fig. 5a). The contact surface is relatively small, and that is probably why, unlike the case of disassembling microtubule tips[31], isolated protofilaments have never been observed under physiological conditions. The protofilament seems to have sufficient stability only in the presence of lateral interactions: parallel in the filament structure and antiparallel in the crystal. A magnified image of the axial interface is shown in Fig. 5b. In the bottom part of the upper subunit, a short segment of the first N-terminal α-helix (Asn 56 to Asp 69) and the unique motif of two consecutive β-turns/β-hairpin (Phe 132 to Asp 151) form a concave surface. In the top part of the lower subunit, a convex surface is formed by short segments of two N-terminal α-helices with a short loop connecting these α-helices (Gln 89 to Asp 107), Leu 408 and Gln 409 of the C-terminal α-helix, and Asn 315 of subdomain D2a. These two surfaces have complementary shapes, which produce a number of van der Waals contacts.

The nature of the interactions is mainly polar–polar or charge–polar. There are two small patches where the interactions are formed between polar and hydrophobic groups, but there are no hydrophobic–hydrophobic interactions. Charge–polar interactions are formed between Asp 69 and Asn 100, Asn 132 and Asp 107, the carbonyl oxygen of Ala 149 and Arg 92, and Asp 151 and Gln 409, of the upper and lower subunit, respectively. Thus, two of the four residues, Ala 149 and Asp 151, are in the short loop at the tip of the β-hairpin of the upper subunit, where Asp 151 is capping the N-terminal end of the C-terminal α-helix of the lower subunit. A portion of the β-hairpin also forms a short intersubunit β-strand with a segment just after the first N-terminal α-helix of the lower subunit. These indicate the important roles of the β-hairpin in domain D1 (Asp 140 to Lys 160) in these axial interactions.

Mechanical switching unit

As discussed above, the protofilament itself is likely to have the ability to switch between the two mechanically stable states with the L- and R-type repeat. As the L-type repeat is only 0.8 Å longer than the R-type, the conformational change would be relatively small. We

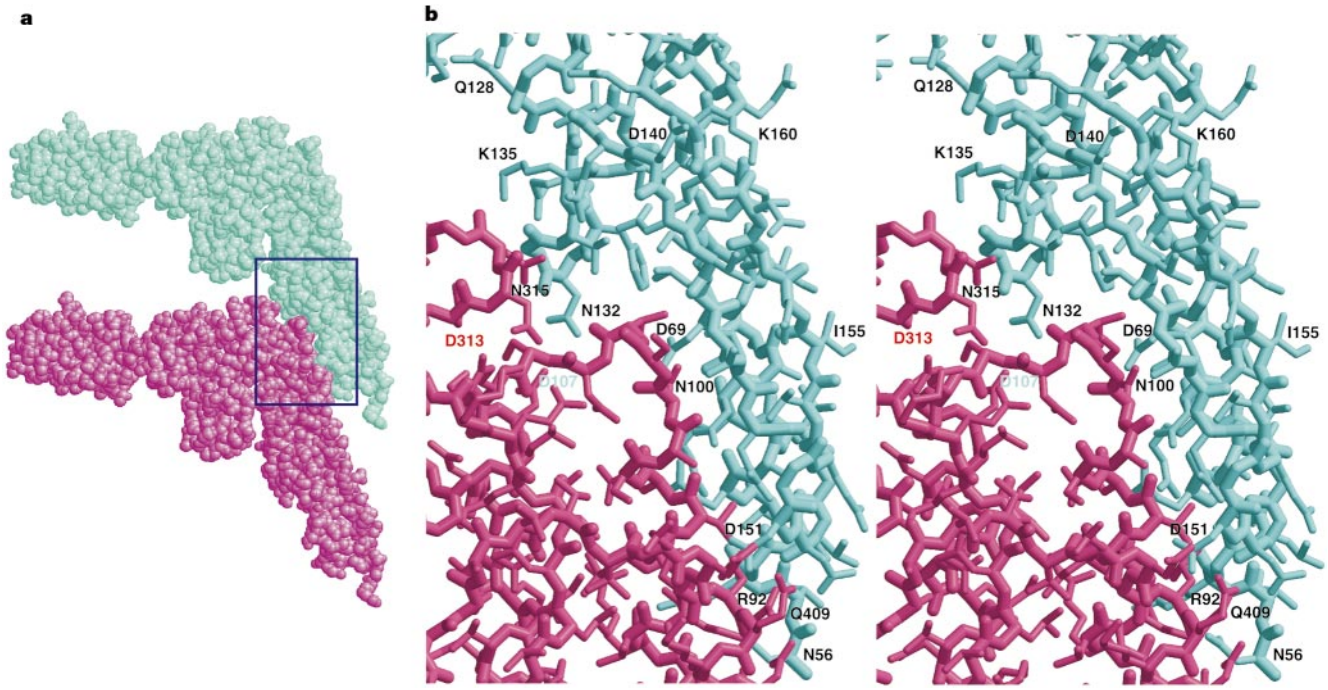

Figure 5 Axial interactions in the protofilament. **a**, Space-filling representation showing the axial packing of two subunits. Prepared with RASMOL[46]. **b**, Stereo close-up view of the boxed region in **a**. The two subunits shown are coloured cyan (upper) and dark pink (lower). Some of the residues are labelled to guide identification. Prepared with MOLSCRIPT[44] and RASTER3D[45].

looked for a local conformational switch in the atomic model of F41 by simulating a gradual extension of the protofilament by fixing its one end and pulling the other end in the axial direction. We used a three-subunit protofilament model, and fixed the top subunit while pulling down the bottom subunit to see what happened in the middle subunit. At every step we translated the bottom subunit by 0.1 Å with its Cα backbone as a rigid body and carried out energy minimization of the model.

The results are shown in Fig. 6. Up to 4.5 Å, every portion of the middle subunit was elastically stretched gradually, as typically shown by the elongating pitch of α-helices (Fig. 6a). But immediately after this point, further translation over the next two steps (0.2 Å) caused an abrupt change in the conformation of the β-hairpin in domain D1, which was accompanied by a small movement of the C-terminal α-helix. Further translation caused further gradual distortion of the molecule as observed before the transition. The two conformations before and after the transition are superimposed for direct comparison in Fig. 6b. The characteristic nature of this switching is a small but significant movement of the β-hairpin that slightly pushes out and down the lower subunit at the axial interface, making the axial subunit dispositions with a longer repeat distance stable.

The two terminal α-helical segments more or less follow the β-hairpin movement, which probably maintains the side-chain interactions with the β-hairpin in the hydrophobic core. Because we carried out the simulated extension with an isolated three-subunit protofilament, without having all those restraints from lateral protofilament packing that are supposed to be present in the filament structure, some of the conformational changes shown here may be artefacts. A more thorough model simulation is needed to prove that the β-hairpin is the switch; however, our current result strongly suggests that the conformational switching of the β-hairpin is responsible for the two distinct states of flagellin packing with two distinct repeat distances at sub-ångstrom accuracy.

Mutations that affect the supercoiling

The amino-acid sequences of flagellin from various bacterial strains show two extremely well conserved regions, which are about 170 residues from the N terminus and about 90 residues from the C terminus (for example, by ProDom domain comparison[32]). From the F41 structure and its position in the filament density, it is clear why these regions are highly conserved. These conserved regions form the densely packed core of the filament—the outer and inner tube (Fig. 4). About a dozen point mutation sites have been identified for a wild-type strain of *S. typhimurium* SJW1103 in relation to the filament morphology[33], and all except one are found within these conserved regions (Fig. 1c). Within F41, mutations D107E, R124A, R124S, G426A and A449V give rise to straight filaments; and mutations D313Y, A414V, A427V, N433D and A449T result in curly filaments (see Fig. 3). We have attempted to interpret the effect of these mutations on the basis of the protofilament structure.

Asp 107 is located at the beginning of the second N-terminal α-helix in the top portion of the lower subunit, and interacts with Asn 132 in the first of the two consecutive β-turns before the β-hairpin in domain D1 of the upper subunit (Fig. 5). The mutant flagellin D107E (from strain SJW1663) forms the L-type straight filament[34]. In the protofilament model, the side chain of Asp 107 points up whereas that of Asn 132 points down, and the distance

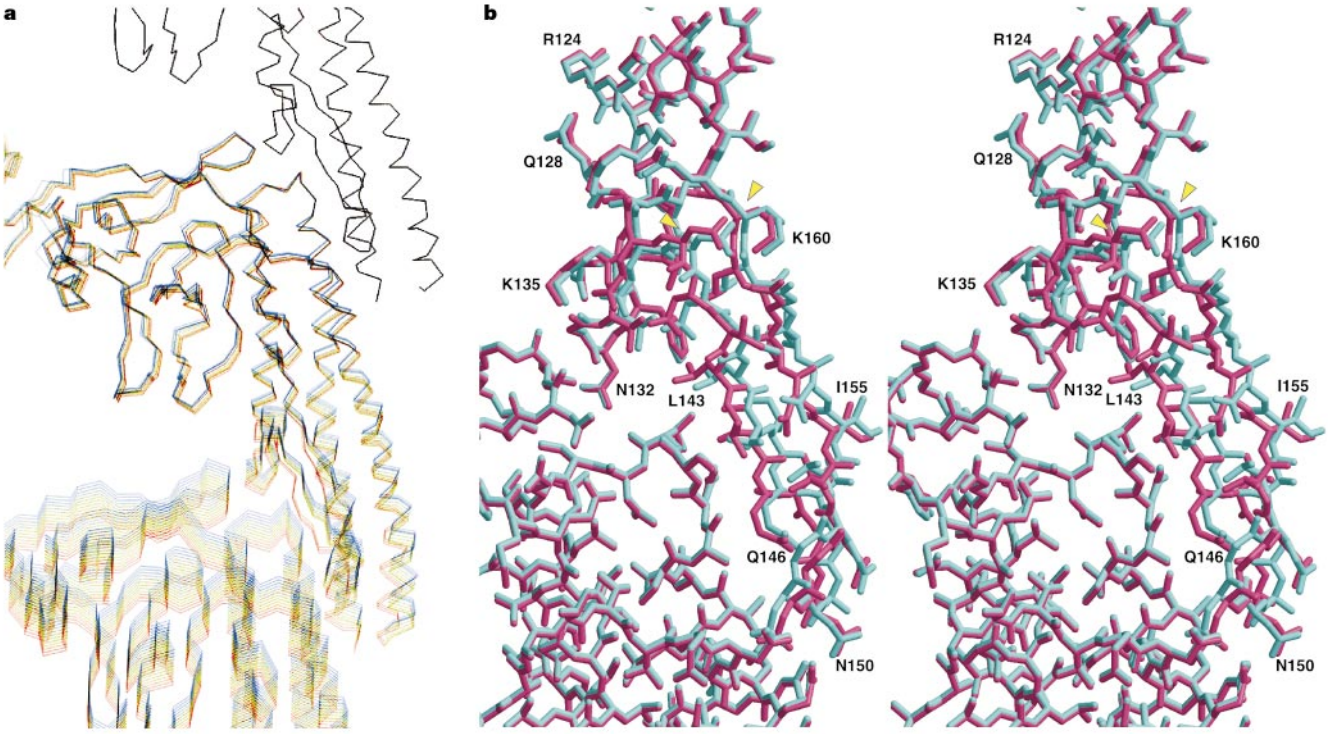

Figure 6 Simulated extension of the protofilament showing the possible switch region. **a**, Superimposition of 12 sampled stages of the simulated extension. Domains D1 and D2 of three F41 molecules are shown (bottom half of the top, whole of the middle, and top half of the bottom) and the 12 stages are colour coded from blue to red. Each step of the extension was 0.1 Å, but every five steps is sampled and displayed here; therefore, the bottom subunits in different stages are equally separated by 0.5 Å. The whole β-hairpin at the bottom of domain D1 of the middle subunit shows a discrete jump in its conformation at an extension from 4.5 to 5.0 Å, whereas other parts show only gradual deformation of an elastic nature. Prepared with O[41]. **b**, Close-up view of the axial contact region in stereo, including the β-hairpin showing the conformational switch. The structures at two sampled stages, at an extension of 4.5 Å in cyan and of 4.7 Å in dark pink, are superimposed to show the conformational switch of the β-hairpin, of which the start and the end are marked by yellow arrowheads. Prepared with MOLSCRIPT[44] and RASTER3D[45].

Table 1 Summary of refinement statistics

Resolution range	No. of reflections with $F > 2\sigma$	No. of residues	No. of protein atoms	No. of water molecules	R_{cryst}*	R_{free}†	r.m.s. bond length	r.m.s. bond angle
10–2.0 Å (2.09–2.0)	29,866 (3,615)	395	2,880	354	23.4% (30.9%)	26.6% (30.8%)	0.009 Å	1.5°

*$R_{cryst} = \Sigma_{hkl}|F_{obs}(hkl) - F_{calc}(hkl)|/\Sigma_{hkl}F_{obs}(hkl)$.
† As R_{cryst}, but calculated on 8% of data set aside for refinement. Numbers in parentheses refer to those in the highest resolution shell.

between them is slightly longer than an average hydrogen bond. Mutation from aspartate to glutamate, which has a slightly longer side chain, would strengthen this hydrogen bond, which may stabilize the conformation of the switch region in the L-state.

Asp 313 is the only mutation located away from the conserved regions, and was previously puzzling. The involvement of this residue is now clearly shown in the structure. Asp 313 is close to Asn 315 in a β-hairpin of subdomain D2a of the lower subunit, where Asn315 makes a hydrogen bond with the main-chain oxygen of Gly 133 of the upper subunit, which is also part of the β-turn to which Asn 132 belongs (Fig. 5). Although not directly, Asp 313 is involved in the axial packing interactions by three portions of the molecule: the β-turn of the upper subunit; the loop between the two N-terminal α-helices; and the tip of the β-hairpin of subdomain D2a of the lower subunit. The mutation D313Y gives rise to curly filaments—one of the right-handed supercoils produced by increasing the number of the R-type protofilaments from two to four or five (a normal filament of wild-type flagellin, a left-handed supercoil, consists of two R-type and nine L-type protofilaments). Because tyrosine has a significantly bulkier side chain than has aspartic acid, this may further stabilize the packing of the three portions in the R-type conformation.

Ala 414 is involved in the hydrophobic core of domain D1 and is close to the short α-helix after the β-hairpin. Its replacement with valine also results in curly filaments, probably through stabilization of the hydrophobic core, which in turn stabilizes the R-type conformation of the switch region.

The other mutated residues do not have any bonding partners within the F41 protofilament; Arg 124 and Ala 427 probably face the lateral neighbours, and Gly 426, Asn 433 and Ala 449 appear to point toward the inner-tube domain, which is missing in the current model. This indicates that the specific form of supercoiling is determined mostly by the lateral interactions between the protofilaments and/or the interactions between the outer- and inner-tube domains.

Conformation of flagellin during transport

For filament growth, flagellin molecules are transported to the distal end of the flagellum through its central channel, which has a diameter of about 30 Å (refs 18, 19). Although there is no data on the conformation of flagellin during the transport, flagellin obviously either has to be unfolded or at least have its domain largely rearranged.

The structure of F41 suggests that, even with intact terminal regions, flagellin is made of independent domains that are connected linearly, and that each domain except for domain D2 is thin enough to fit inside the channel. Therefore, it may be sufficient to have partially unfolded domain D2 and flexible interdomain connections during the transport. If flagellin comes out of the flagellum through the opening under the cap at the distal end[35] in the order of D3 first followed by D2 and D1, it would be ideal for a rapid self-assembly process. This question remains to be answered by experimental data.

Towards construction of the filament model

The structure of the flagellar protofilament has provided many insights into the structural mechanism of flagellin polymerization and the possible switch region responsible for the two-state mechanical switch of sub-ångstrom precision, which defines the curvatures of the supercoiled flagellar filaments. However, understanding the mechanisms that determine a particular twist of a supercoil and its dynamic switching between left- and right-handed ones, for example by the twisting force produced by rapid motor reversal, requires detailed analyses of the lateral packing interactions between the protofilaments in the filament structure.

The approximate models of the L- and R-type straight filaments produced by docking the protofilament model into low-resolution density maps with slight deformations are not sufficient, because the switching in the lateral interactions is a mutual sliding over a few ångstroms[17]. To identify correctly the atomic interactions involved in the switching, we are now incorporating experimental data obtained from electron cryomicroscopy and X-ray fibre diffraction with those obtained from X-ray crystallography to construct accurate models of the L- and R-type straight filaments. □

Methods

F41 preparation and crystallization

The F41 fragment of flagellin from *Salmonella typhimurium* was prepared and crystallized as described[23]. Briefly, crystals were grown in solutions containing 6% PEG-6000, 12% glycerol, 3–6% isopropanol, 50–75 mM NaCl, 20 mM Tris-HCl, pH 7.8, at 16 °C. Glycerol and isopropanol were important in reducing the otherwise very high nucleation rate, which resulted in many micrometre-sized needle crystals[23].

Data collection

The space group of the crystal was $P2_1$, with the cell dimensions $a = 51.8$, $b = 36.5$, $c = 118.7$ Å, $\beta = 90.8°$. The solvent content was about 55% and the crystal contained one molecule per asymmetric unit. The size of the F41 crystal was typically 0.5 mm × 0.2 mm × <0.01 mm, which made data collection difficult. The crystals were frozen in liquid propane and routinely annealed in the cryostream to improve the diffraction at high resolution[23]. All the data sets were collected at temperatures around 100 K. Because of the long exposure time (5 h per frame) required to record high-resolution spots, even with the high-brilliance X-ray beam of our in-house Rigaku X-ray oscillation camera (fine focus X-ray generator, FR-D; Yale-type optics; image plate detector, RAXIS-IV), only well-diffracting crystals were selected in the laboratory, and full data sets were collected at synchrotron beam lines. Data sets used for the structure analysis are listed in the Supplementary Information.

A set of multi-wavelength anomalous diffraction (MAD) data, which produced a high-quality electron density map at 2.0 Å resolution, were collected under Trichromatic concept[36] at RIKEN beamline I (BL45XU) at the 8 GeV Super Photon ring (SPring-8) in Harima[37]. The data were reduced by DENZO and SCALEPACK[38], or MOSFLM[39] and SCALA[40]. The atomic model was built as shown in the Supplementary Information. The model was refined at 2.0 Å resolution including 354 water molecules (Table 1).

Structure analysis

Because the F41 crystals prepared from three different flagellins (wild type, L-type, and G365C mutant of the R-type) all showed the same cell dimensions within experimental errors, we treated them as isomorphous crystals. An electron density map was first obtained at 2.5 Å resolution by multiple isomorphous replacement using two derivative data sets (L57 and C77; see Supplementary Information). We traced the main chain in domain D1 using the graphics program O[41], but it was difficult to complete the model building. Then, we obtained new phases to 2.0 Å using a set of MAD data (G19; see Supplementary Information) and program SOLVE[42], which enabled us to complete the model building. The N-terminal three residues are not included in the model because that part of electron density was obscure. We then refined the atomic model, comprising 395 amino-acid residues and 354 water molecules, against the data collected at ESRF ID14-3 by using X-PLOR[43] (see Table 1). We also refined the model against three data sets obtained from the F41 crystals prepared from three different flagellins, but could not find any significant difference between the three, which we will describe and discuss in more detail elsewhere.

Simulated extension of the protofilament

Simulation of the protofilament extension was carried at every 0.1 Å step by energy minimization of the three-subunit protofilament model with Cα atoms of both top and

bottom subunits treated as rigid bodies. We used a routine in X-PLOR[43] for energy minimization.

Received 2 November 2000; accepted 11 January 2001.

1. Berg, H. C. & Anderson, R. A. Bacteria swim by rotating their flagellar filaments. *Nature* **245,** 380–382 (1973).
2. Silverman, M. & Simon, M. Flagellar rotation and the mechanism of bacterial motility. *Nature* **249,** 73–74 (1974).
3. Kudo, S., Magariyama, Y. & Aizawa, S.-I. Abrupt changes in flagellar rotation observed by laser dark-field microscopy. *Nature* **346,** 677–680 (1990).
4. Ryu, W. S., Berry. R. M. & Berg, H. C. Torque-generating units of the flagellar motor of *Escherichia coli* have a high duty ratio. *Nature* **403,** 444–447 (2000).
5. Larsen, S. H., Reader, R. W., Kort, E. N., Tso, W. W. & Adler, J. Change in direction of flagellar rotation is the basis of the chemotactic response in *Escherichia coli*. *Nature* **249,** 74–77 (1974).
6. Macnab, R. M. & Ornston, M. K. Normal-to-curly flagellar transitions and their role in bacterial tumbling. Stabilization of an alternative quaternary structure by mechanical force. *J. Mol. Biol.* **112,** 1–30 (1977).
7. Turner, L., Ryu, W. S. & Berg, H. C. Real-time imaging of fluorescent flagellar filaments. *J. Bacteriol.* **182,** 2793–2801 (2000).
8. O'Brien, E. J. & Bennett, P. M. Structure of straight flagella from a mutant *Salmonella*. *J. Mol. Biol.* **70,** 133–152 (1972).
9. Asakura, S. Polymerization of flagellin and polymorphism of flagella. *Adv. Biophys. (Japan)* **1,** 99–155 (1970).
10. Calladine, C. R. Construction of bacterial flagella. *Nature* **225,** 121–124 (1975).
11. Calladine, C. R. Design requirements for the construction of bacterial flagella. *J. Theor. Biol.* **57,** 469–489 (1976).
12. Calladine, C. R. Change of waveform in bacterial flagella: The role of mechanics at the molecular level. *J. Mol. Biol.* **118,** 457–479 (1978).
13. Kamiya, R. & Asakura, S. Helical transformations of *Salmonella* flagella *in vitro*. *J. Mol. Biol.* **106,** 167–186 (1976).
14. Kamiya, R. & Asakura, S. Flagellar transformations at alkaline pH. *J. Mol. Biol.* **108,** 513–518 (1977).
15. Hotani, H. Micro-video study of moving bacterial flagellar filaments III. Cyclic transformation induced by mechanical force. *J. Mol. Biol.* **156,** 791–806 (1982).
16. Kamiya, R., Asakura, S., Wakabayashi, K. & Namba, K. Transition of bacterial flagella from helical to straight forms with different subunit arrangements. *J. Mol. Biol.* **131,** 725–742 (1979).
17. Yamashita, I. *et al.* Structure and switching of bacterial flagellar filament studied by X-ray fiber diffraction. *Nature Struct. Biol.* **5,** 125–132 (1998).
18. Mimori, Y. *et al.* The structure of the R-type straight flagellar filament of *Salmonella* at 9 Å resolution by electron cryomicroscopy. *J. Mol. Biol.* **249,** 69–87 (1995).
19. Morgan, D. G., Owen, C., Melanson, L. A. & DeRosier, D. J. Structure of bacterial flagellar filaments at 11 Å resolution: Packing of the α-helices. *J. Mol. Biol.* **249,** 88–110 (1995).
20. Mimori-Kiyosue, Y., Vonderviszt, F., Yamashita, I., Fujiyoshi, Y. & Namba, K. Direct interaction of flagellin termini essential for polymorphic ability of flagellar filament. *Proc. Natl Acad. Sci. USA* **93,** 15108–15113 (1996).
21. Mimori-Kiyosue, Y., Vonderviszt, F. & Namba, K. Locations of terminal segments of flagellin in the filament structure and their roles in polymerization and polymorphism. *J. Mol. Biol.* **270,** 222–237 (1997).
22. Mimori-Kiyosue, Y., Yamashita, I., Fujiyoshi, Y., Yamaguchi, S. & Namba, K. Role of the outermost subdomain of *Salmonella* flagellin in the filament structure revealed by electron cryomicroscopy. *J. Mol. Biol.* **284,** 521–530 (1998).
23. Samatey, F. A., Imada, K., Vonderviszt, F., Shirakihara, Y. & Namba, K. Crystallization of the F41 fragment of flagellin and data collection from extremely thin crystals. *J. Struct. Biol.* **132,** 106–111 (2000).
24. Vonderviszt, F., Uedaira, H., Kidokoro, S. -I. & Namba, K. Structural organization of flagellin. *J. Mol. Biol.* **214,** 97–104 (1990).
25. Honda, S., Uedaira, H., Vonderviszt, F., Kidokoro, S. -I. & Namba, K. Folding energetics of a multidomain protein, flagellin. *J. Mol. Biol.* **293,** 719–732 (1999).
26. Yoshioka, K., Aizawa, S. -I. & Yamaguchi, S. Flagellar filament structure and cell motility of *Salmonella typhimurium* mutants lacking part of the outer domain of flagellin. *J. Bacteriol.* **177,** 1090–1093 (1995).
27. Nogales, E., Sharon, G. W., & Downing, K. H. Structure of the αβ tubulin dimer by electron crystallography. *Nature* **391,** 199–203 (1998).
28. Yamashita, I. *et al.* Radial mass analysis of the flagellar filament of *Salmonella*: Implications for subunit folding. *J. Mol. Biol.* **253,** 547–558 (1995).
29. Namba, K., Yamashita, I. & Vonderviszt, F. Structure of the core and central channel of bacterial flagella. *Nature* **342,** 648–654 (1989).
30. Vonderviszt, F., Aizawa, S. -I. & Namba, K. Role of the disordered terminal regions of flagellin in filament formation and stability. *J. Mol. Biol.* **221,** 1461–1474 (1991).
31. Mandelkow, E. -M., Mandelkow, E. & Milligan, R. A. Microtubule dynamics and microtubule caps: A time-resolved cryo-electron microscopy study. *J Cell Biol.* **114,** 977–991 (1991).
32. Corpet, F., Gouzy, J. & Kahn, D. The ProDom database of protein domain families. *Nucleic Acids Res.* **26,** 323–326 (1998).
33. Kanto, S, Okino, H., Aizawa, S. -I. & Yamaguchi, S. Amino acids responsible for flagellar shape are distributed in terminal regions of flagellin. *J. Mol. Biol.* **219,** 471–480 (1991).
34. Kamiya, R., Asakura, S. & Yamaguchi, S. Formation of helical filaments by copolymerization of two types of 'straight' flagellins. *Nature* **286,** 628–630 (1980).
35. Yonekura, K. *et al.* The bacterial flagellar cap as the rotary promoter of flagellin self-assembly. *Science* **290,** 2148–2152 (2000).
36. Yamamoto, M., Kumasaka, T., Fujisawa, T. & Ueki, T. Trichromatic concept at Spring-8 RIKEN beamline I. *J. Synchrotron Rad.* **5,** 222–225 (1998).
37. Ueki, T. & Yamamoto, M. The start of a new generation: the present status of the Spring-8 synchrotron and its use in structural biology. *Structure* **7,** R183–R187 (1999).
38. Otwinowski, Z. & Minor, W. *Processing of X-ray Diffraction Data Collected in Oscillation Mode* (Academic, New York, 1997).
39. Leslie, A. G. W. CCP4/ESF-EACMB. *Newslett. Protein Crystallogr.* Vol. 26 (Daresbury Laboratory, Warrington, UK, 1992).
40. Collaborative Computational Project Number 4. The CCP4 suite: Programs for protein crystallography. *Acta Crystallogr. D* **50,** 760–763 (1994).
41. Jones, T. A., Zhou, J. Y., Cowan, S. W. & Kjeldgaard, M. Improved methods for building protein models in electron density maps and the location of errors in these models. *Acta Crystallogr. A* **47,** 110–119 (1991).
42. Terwilliger, T. C. & Berendzen, J. Automated structure solution for MIR and MAD. *Acta Crystallogr. D* **55,** 849–861 (1999).
43. Brünger, A. T., Kuriyan, J. & Karplus, M. Crystallography R factor refinement by molecular dynamics. *Science* **235,** 458–460 (1987).
44. Kraulis, P. J. MOLSCRIPT: a program to produce both detailed and schematic plots of protein structures. *J. Appl. Crystallogr.* **24,** 946–950 (1991).
45. Merritt, E. A. & Bacon, D. J. Raster3D: Photorealistic molecular graphics. *Methods Enzymol.* **277,** 505–524. (1997).
46. Sayle, R. A. & Milner-White, E. J. RasMol: Biomolecular graphics for all. *Trends Biochem. Sci.* **20,** 374–376 (1995).

Supplementary information is available on *Nature*'s World-Wide Web site (http://www.nature.com) or as paper copy from the London editorial office of *Nature*.

Acknowledgements

We thank T. Tomizaki, L. Dumon, W. Burmeister, S. Arzt and S. Wakatsuki at ESRF, and M. Kawamoto, N. Kamiya and K. Miura at SPring-8 for technical help with beamlines. We also thank I. Yamashita and K. Hasegawa for a mutant strain of *Salmonella* that produces SJW1655-derived site-directed mutant flagellin (G365C), which forms the R-type straight flagellar filament, and helpful information of heavy-atom binding to the filament; J. Tame for critically reading the manuscript; and S. Asakura, T. Nitta and F. Oosawa for continuous support and encouragement.

Correspondence and requests for materials should be addressed to K.N. (e-mail: keiichi@crl.mei.co.jp). Atomic coordinates have been deposited in the Protein Data Bank under accession code 1IO1.